

Experimental realization of 105-qubit random access quantum memory

N. Jiang^{1*}, Y.-F. Pu^{1*†}, W. Chang¹, C. Li¹, S. Zhang¹, L.-M. Duan^{‡1}

¹*Center for Quantum Information, IIIS, Tsinghua University, Beijing 100084, PR China*

Random access memory is an indispensable device for classical information technology. Analog to this, for quantum information technology, it is desirable to have a random access quantum memory with many memory cells and programmable access to each cell. We report an experiment that realizes a random access quantum memory of 105 qubits carried by 210 memory cells in a macroscopic atomic ensemble. We demonstrate storage of optical qubits into these memory cells and their read-out at programmable times by arbitrary orders with fidelities exceeding any classical bound. Experimental realization of a random access quantum memory with many memory cells and programmable control of its write-in and read-out makes an important step for its application in quantum communication, networking, and computation.

INTRODUCTION

Classical random access memory, with its programmable access to many memory cells and site-independent access time, has found wide applications in information technologies. Similarly, for realization of quantum computational or communicational networks, it is desirable to have a random access quantum memory (RAQM) with the capability of storing many qubits, individual addressing of each qubit in the memory cell, and programmable write-in and read-out of the qubit from the memory cell to a flying bus qubit with site-independent access time [1–10]. Such a device is useful for both quantum communication and computation [1–10]. It provides a key element for realization of long-distance quantum communication through the quantum repeater network [1–7]. The write-in and read-out operations require implementation of a good quantum interface between the bus qubits, typically carried by the photonic pulses, and the memory qubits, which are usually realized with the atomic spin states. A good quantum interface should be able to faithfully map quantum states between the memory qubits and the bus qubits. A convenient implementation of the quantum interface is based on the directional coupling of an ensemble of atoms with the forward propagating signal photon pulse induced by the collective enhancement effect [2–6, 11]. A number of experiments have demonstrated this kind of quantum interfaces and their applications both in the atomic ensemble [11–23] and the solid-state spin ensemble with a low-temperature crystal [24–29].

To scale up the capability of a quantum memory, which is important for its application, an efficient method is to use the memory multiplexing, based on the use of multiple spatial modes [17, 20], or temporal modes [25, 26, 28, 29], or angular directions [21] within a single atomic or solid-state ensemble. Through multiplexing of spatial modes, recent experiments have realized a dozen to hundreds of memory cells in a single atomic ensemble, however, write-in and read-out of external quantum signals have not been demonstrated yet [17, 20]. With temporal multiplexing, a sequence of time-bin qubits have been stored into a solid-state ensemble, however, the whole pulse sequence needs to be read out together with a fixed order and interval between the pulses for lack of individual addressing [26, 28, 29]. It remains a challenge to demonstrate a RAQM with programmable and on-demand control to write-in and read-out of each individual quantum signals stored into the memory cells.

In this paper, we demonstrate a RAQM which can store 105 qubits in its 210 memory cells using the dual-rail representation of a qubit. A pair of memory cells stores the state of the input photonic qubit, which is carried by the two paths of a very weak coherent pulse. We have measured the fidelities and the efficiencies for the write-in, storage, and readout operations for all the 105 pairs of memory cells. The fidelities, typically around or above 90%, are significantly higher than the classical bound and therefore confirm quantum storage. To demonstrate the key random access property, we show that different external optical qubits can be written into the multi-cell quantum memory, stored there simultaneously, and read out later on-demand by any desired order with the storage time individually controlled for each qubit. The fidelities for all the qubits still significantly exceed the classical bound with negligible crosstalk errors between them.

* These authors contributed equally to this work.

† Present address: Institute for Experimental Physics, University of Innsbruck, A-6020 Innsbruck, Austria

‡ Corresponding author: lmduan@tsinghua.edu.cn

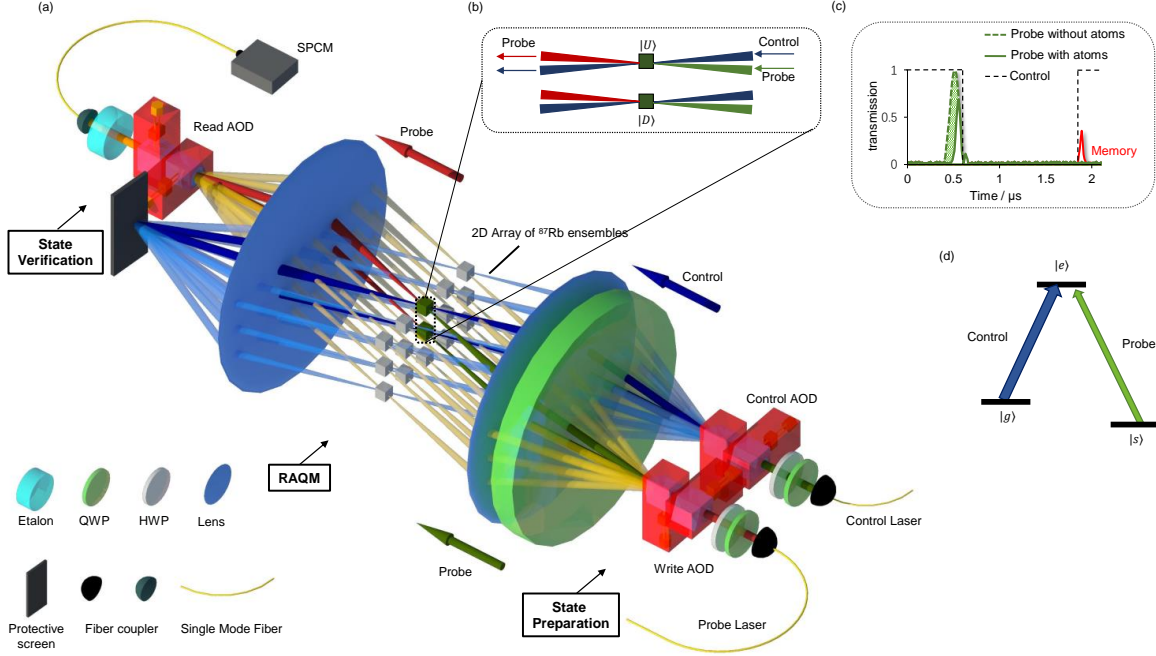


FIG. 1: **Experimental setup for realization of a multiplexed random access quantum memory with a macroscopic atomic ensemble.** (a) We use two-dimensional (2D) AODs to control the multiplexing of control and probe beams which are coupled to a macroscopic atomic ensemble under the EIT configuration. The qubit state of the probe photon is stored into a pair of memory cells using the dual-rail representation and later retrieved for read out after a controllable storage time. Through programming the AODs, we individually address and control a 2D array of 15×14 atomic memory cells (for clarity only 3×5 cells are shown in the figure), which can store 105 optical qubits. The lens, set in a $4f$ -configuration, are used to focus the beams as well as to map different angles of the deflected beams after the AODs to different micro-ensembles in the 2D array. We use a Fabry-Perot cavity (etalon) in the path of the retrieved photon for frequency filtering of the leaked control light. The write AOD prepares the input state for the atomic memory, where the optical qubit is carried by superposition of different optical paths. This input state, unknown to the atomic memory, is stored into the multi-cell atomic ensemble. After a controllable storage time, this state is mapped out to the optical state carried by different optical paths (on the left side of the atomic ensemble) and verified in complementary qubit bases by a combination of the read AOD and the SPCM (single-photon counting module). (b) Zoom-in of the beam configuration at two memory cells denoted as U and D for qubit storage. (c) Histogram of the time-resolved photon counts for the transmitted probe light registered by the single-photon detector. The solid (dashed) green curves represent respectively the probe pulse with (without) the MOT atoms, and their difference corresponds to the stored photon component. The red curve represents the retrieved photon pulse after a controllable storage time. (d) The energy levels of the ^{87}Rb atoms coupled to the control and the probe beams through the EIT configuration, with $|g\rangle \equiv |5S_{1/2}, F=2\rangle$, $|s\rangle \equiv |5S_{1/2}, F=1\rangle$, $|e\rangle \equiv |5P_{1/2}, F'=2\rangle$.

RESULTS

Experimental setup

Our experimental setup is illustrated in Fig. 1. The macroscopic atomic ensemble is realized with a cloud of ^{87}Rb atoms trapped and cooled down by a magneto-optical trap (MOT) (see Supplementary Note 1). We divide this macroscopic ensemble into a two-dimensional (2D) array of 15×14 micro-ensembles. Each micro-ensemble is individually addressed through a pair of crossed acoustic optical deflectors (AODs) inserted into the paths of the control beam, the input probe beam, and the output probe beam (see Supplementary Note 2). The AODs provide a convenient device for multiplexing and de-multiplexing of many different optical paths, which have been used recently to control neutral atoms [17, 20, 30] as well as trapped ions [31]. The relative phases between those 210 different optical paths are intrinsically stable as the beams along different paths go through the same optical devices.

The atoms in the whole ensemble are initially prepared to the state $|g\rangle \equiv |5S_{1/2}, F=1\rangle$ through optical pumping and the MOT is turned off right before the quantum memory experiment. For each micro-ensemble, the probe and the control beams are interacting through the electromagnetically-induced transparency (EIT) configuration shown

in Fig. 1 [11], where an incoming photon in the probe beam is converted by the control beam (the write pulse) to a collective spin wave excitation in the level $|s\rangle \equiv |5S_{1/2}, F=2\rangle$ through the excited state $|e\rangle \equiv |5P_{1/2}, F'=2\rangle$. The write pulse is then shut off. After a programmable storage time in the quantum memory, the excitation in the spin wave mode is converted back to an optical excitation in the output probe beam by shining another pulse (the read pulse) along the control beam direction.

Characterization of storage fidelities for every memory cells

The input qubit state is carried by two optical paths $|U\rangle$ and $|D\rangle$ of a photon, and any superposition state $c_0|U\rangle + c_1|D\rangle$ with arbitrary coefficients c_0, c_1 can be generated and controlled through the input AODs. The input signal is carried by a very weak coherent pulse with the mean photon number $\bar{n} \simeq 0.5$. In our proof-of-concept experiment, the input state for the atomic memory is prepared by the write AODs as illustrated in Fig. 1(a). This pair of AODs can split the weak coherent signal into arbitrary superpositions along two different optical paths, and the single-photon component of this weak signal represents the effective qubit state, with the qubit information carried by the superposition coefficients along the different optical paths. Note that the input qubit state, prepared by the write AODs, remains unknown to the atomic ensemble which acts as the multiplexed quantum memory in this experiment. This dual-rail encoding of qubit is same as the path or polarization qubit used in many optical quantum information experiments, where the single-photon component of a very weak coherent state carries the qubit state and is selected out by the single-photon detectors afterwards.

Similar to other optical quantum information experiments [2–6], we use two quantities—conditional fidelity and efficiency—to characterize the imperfections of a quantum memory. The conditional fidelity characterizes how well the qubit state is preserved when a photon is registered on the output channel after its storage in the quantum memory [32]. The (intrinsic) efficiency characterizes the success probability of a stored photon reappeared in the output single-mode fiber after a certain storage time. For application of quantum memory in quantum information protocols, such as for implementation of quantum repeaters [1–3, 6], the conditional fidelity is typically the most important figure-of-merit as it determines the fidelity of the overall protocol and characterizes whether one can enter the quantum region by beating the classical bound. The efficiency influences the overall success probability of the quantum information protocol. For the quantum repeater protocol based on the DLCZ (Duan-Lukin-Cirac-Zoller) scheme [2, 3, 6], the scaling of required resources remains polynomial at any finite efficiency, but the scaling exponent gets significantly less when one increases the efficiency. For quantum memory experiments, one needs to first achieve a high enough conditional fidelity to prove that the system enters the quantum storage region by beating the classical bound and then improve the efficiency as much as one can.

The input optical qubit is stored into a pair of neighboring micro-ensembles through the EIT process and then retrieved after a programmable storage time by controlling the write/read pulses in the corresponding paths. The write/read pulses are delivered to different paths through the control AODs. Our atomic quantum memory with a 2D array of 15×14 memory cells has the capability to store 105 optical qubits as shown in Fig. 2a. First, we measure the storage fidelity for each pair of the memory cells one by one by inputting an optical qubit and then retrieving it for readout after a storage time of $1.38 \mu\text{s}$. The output qubit state is measured through quantum state tomography [33] by using the output AODs to choose the complementary detection bases. The experimentally reconstructed density operator ρ_o is compared with the input state $|\Psi_{in}\rangle$ prepared by the input AODs to get the storage fidelity $F = \langle \Psi_{in} | \rho_o | \Psi_{in} \rangle$. For each pair of the memory cells, we measure the storage fidelity F under six complementary input states with $|\Psi_{in}\rangle$ taking $|U\rangle, |D\rangle, |\pm\rangle = (|U\rangle \pm |D\rangle)/\sqrt{2}$, and $|\sigma_{\pm}\rangle = (|U\rangle \pm i|D\rangle)/\sqrt{2}$, and the results are shown in Fig. 2b for all the 105 pairs of memory cells. The averaged conditional fidelity \bar{F} , from the above six measurements with equal weight, is shown in Fig. 2c. For a single-photon input state, the classical bound (maximum value) for the conditional storage fidelity \bar{F} is $2/3$ (see the Supplement). When we consider the contribution of small multi-photon components in the weak coherent pulse (with $\bar{n} \simeq 0.5$), the classical bound is raised to 68.8% (see Supplementary Note 3 and [27, 29, 34]). Our measured conditional fidelities \bar{F} for those 105 pairs of memory cells are above or around 90%. The average of the conditional fidelities over the 105 pairs is $(94.45 \pm 0.06)\%$. The standard deviations of these measurements are shown in the Supplementary Note 4. The measured conditional fidelities for all the memory cells significantly exceed the classical bound by more than four standard deviations.

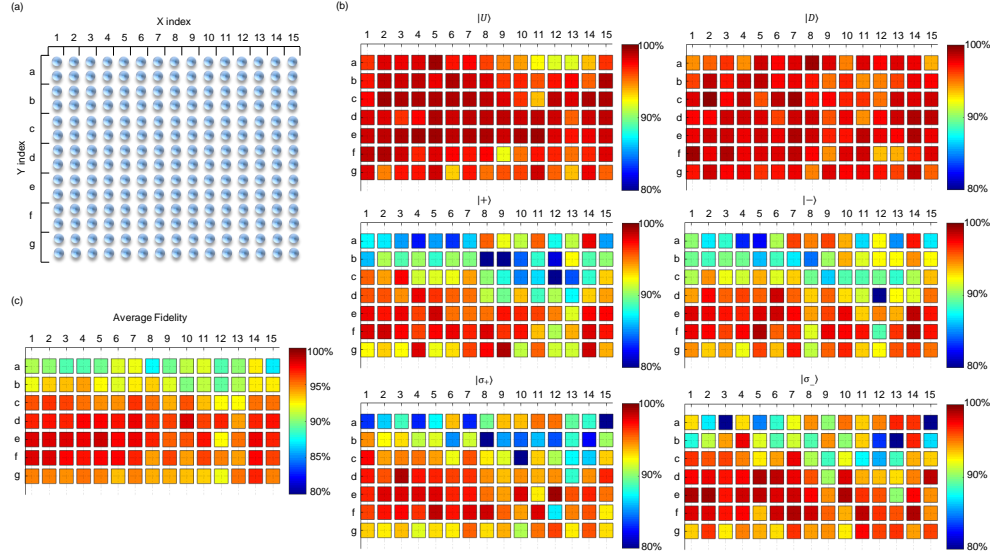


FIG. 2: Measured state fidelities of the retrieved optical qubits after storage in the 210-cell quantum memory. (a) Illustration of the 105-qubit quantum memory. Each qubit is carried by a pair of neighboring memory cells in the 2D array. (b) Quantum state fidelities measured for the six complementary input states of optical qubits after a $1.38 \mu\text{s}$ storage time. We measured the fidelities for all the 105 pairs of memory cells one by one. (c) The average storage fidelities for the 105 pairs of memory cells.

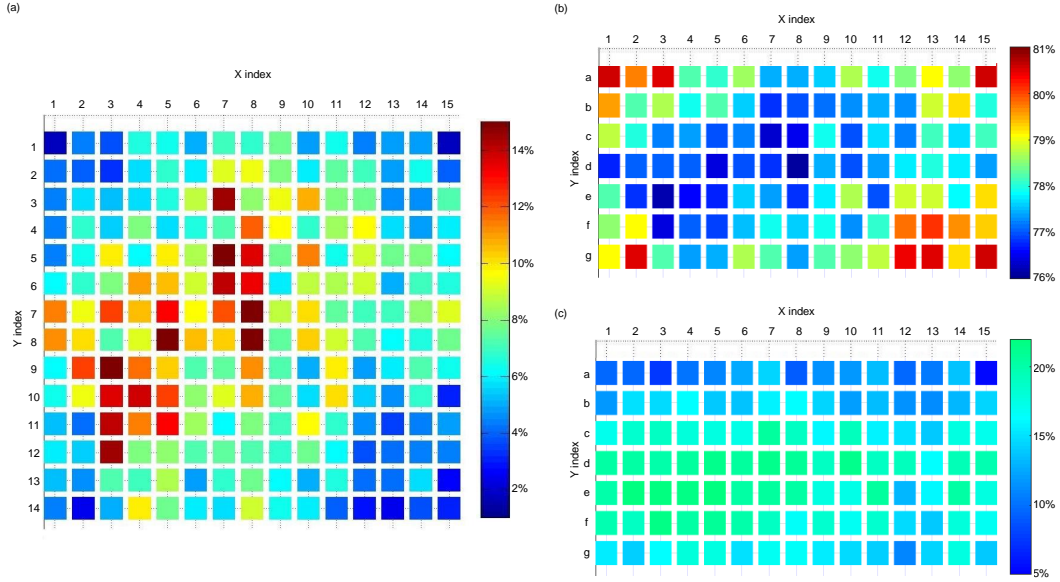


FIG. 3: Photon retrieval efficiency from the memory cells and its influence on the classical bound of the storage fidelity. (a) Photon retrieval efficiency measured for the 2D array of 15×14 memory cells. The storage time here is $1.38 \mu\text{s}$. (b) The classical bound on the storage fidelity for each pair of memory cells, taking into account of the retrieval efficiency and the multi-photon components. (c) The measured storage fidelities subtracted by the corresponding classical bounds. The positive values indicate that we have demonstrated quantum storage for every pairs of memory cells.

Characterization of storage efficiencies and efficiency-dependent classical bounds

We then measure the efficiency of the photon storage in each memory cell. The measurement is done by directing the weak coherent pulse (with $\bar{n} \simeq 0.5$) to each memory cell and then detect the probability of the stored photon going to the output single-mode fiber after a storage time of $1.38 \mu\text{s}$. The detection is scanned over all the memory cells by controlling the optical paths with the set of input and output AODs. The results are shown in Fig. 3a. The efficiency

ranges from 18% for the middle memory cells to about 2% for the edge memory cells. The major contributor to this inefficiency is the limited optical depth of the atomic cloud, which is about 5 at the center of the array and decreases to below 1 at the edge. According to theory, the intrinsic efficiency can be significantly improved with moderate increase of the optical depth [35]. Very recent experiments have demonstrated impressively high intrinsic efficiencies for both strong classical pulse [22] and weak coherent pulse [23]. This is achieved by a significant increase of the optical depth of the atomic ensemble through use of elongated 2D (two-dimensional) MOT or compressed MOT. As the 2D or compressed MOT has a small cross section, it is not straightforward to extend the techniques in those experiment to allow the spatial multiplexing for realization of multi-cell quantum memories. However, those experiments [22, 23], together with the theoretical calculation in Ref. [35], demonstrates that a large improvement in the intrinsic efficiency is possible by a reasonable increase of the optical depth of the atomic cloud. To have a larger optical depth and at the same time a larger cross section for spatial multiplexing, one way is to prepare a larger MOT by loading of pre-cooled atoms into the memory MOT, using the double MOT structure or an additional Zeeman slower. Alternatively, we can also try to decrease the waist diameters of the control/probe beams so that each memory cell takes a smaller cross section in the whole atomic ensemble. Eventually, it would be desirable to load the atoms into 2D arrays of far-off-resonance optical traps to increase the memory time as well as to make the optical depth more homogeneous for all the memory cells.

When we take into account the contribution of the inefficiency of the quantum storage, the classical bound for the conditional storage fidelity will be increased [27]. In Fig. 3b, we show the calculated classical fidelity bound for each pair of memory cells (see Supplementary Note 3), taking into account the contributions of both the multi-photon components in a weak coherent pulse and the measured inefficiencies for the corresponding cells. Our measured storage fidelities for all the 105 pairs of memory cells shown in Fig. 2c are still higher than the corresponding classical bounds. To compare, in Fig. 3c we show the difference in values between the measured conditional fidelity and the corresponding classical bounds. All the values are positive, and all of them exceed the classical bound by at least four standard deviations. The minimum difference is 6.4% here, about 4 standard deviations above the classical bound. This confirms that we have demonstrated quantum storage for all the 105 qubits in this multi-cell memory after taking into account of the experimental imperfections.

Demonstration of random access quantum storage

Now we demonstrate the random access feature of this quantum memory. By programming the AODs to control the optical paths, we can write multiple photonic qubits into any of those memory cells and read them out later on-demand by an arbitrary order. To experimentally verify this, we store three qubits into three pairs of memory cells shown in Fig. 4a, in the order of qubits 1-2-3. After a controllable storage time, we read out these qubits in a programmable way by three different orders. The control sequences for the write-in and readout process are shown in Fig. 4b and can be fully programed. In Fig. 4c, we show the storage fidelity measured through quantum state tomography, the retrieval efficiency, and the storage time for each qubit, with three different readout orders of qubits 1-2-3, 3-2-1, and 2-1-3. All the fidelities exceed the corresponding classical bounds, even after taking into account of the multi-photon components and the storage inefficiencies. The above control methods for three qubits can be similarly applied for simultaneous storage of more qubits and programing of their readout patterns. The current experiment is mainly limited by the memory time in the atomic ensemble, which is about $27.8 \mu s$ ($1/e$ decay time), caused by the thermal motion of the atomic gas and the remaining small magnetic field gradient. The memory time in the atomic ensemble can be extended by orders of magnitude if we make use of a far-of-resonant optical trap to confine the atoms [18, 19].

DISCUSSION

Our experiment realizes a multiplexed random access quantum memory with 210 memory cells that can store 105 optical qubits. We demonstrate programmable storage and readout of individual qubits in the memory cells with the access time and the readout order fully controllable and independent of the physical location of the cells. This random access feature, together with the large capacity for storing optical qubits in a single macroscopic ensemble, opens up an interesting perspective for applications. For instance, it could be useful for realization of multiplexed quantum repeater networks towards long-distance communication and quantum internet [1–7] or for optical quantum information processing and computation that requires the memory components [8–10]. The random access control

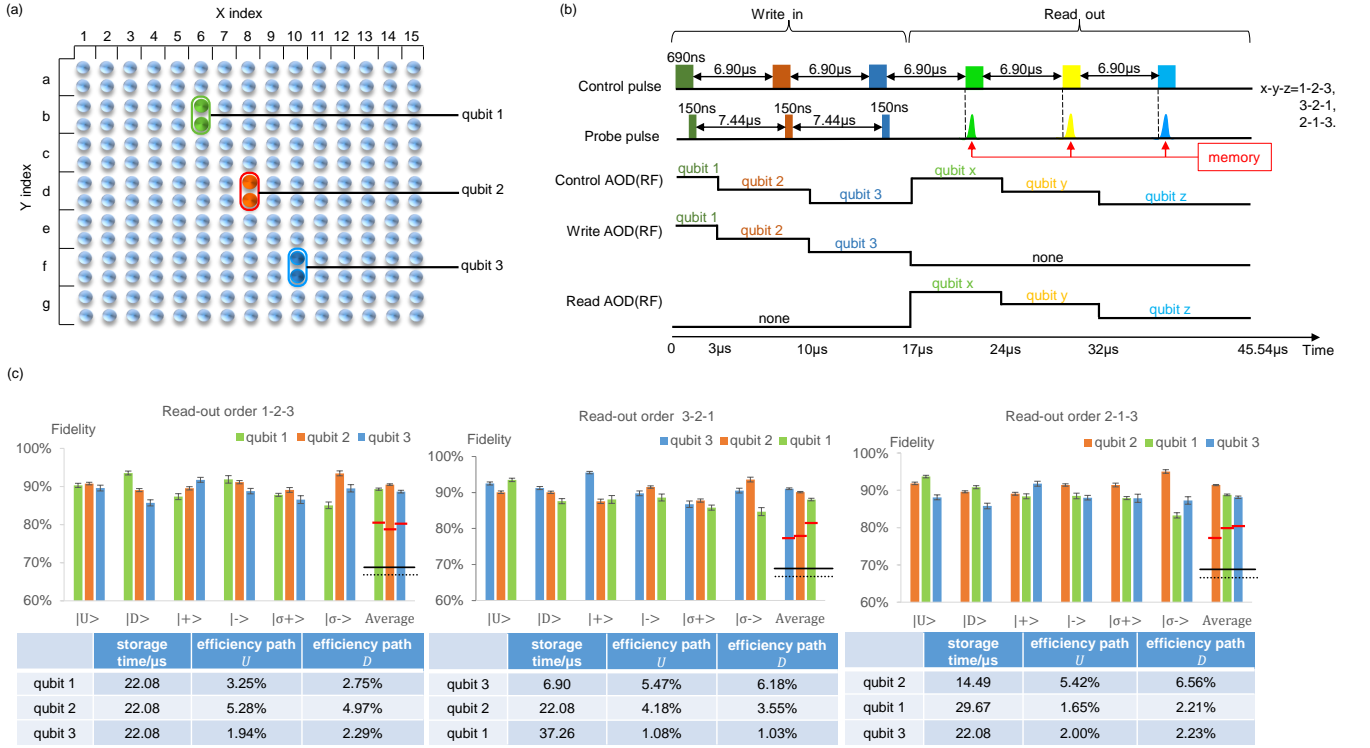


FIG. 4: Demonstration of the random access feature for the multi-cell quantum memory. (a) The positions of the three pairs of memory cells in the 2D array that we choose in this demonstration. (b) The time sequences for the control pulse, the probe pulse, the radio-frequency (RF) signals that drive the control AODs, the write AODs, and the read AODs. Different heights of the RF signals mean that the corresponding AODs choose different pairs of memory cells for individual addressing and control. (c) The measured state fidelities of the three qubits stored into the corresponding atomic memory cells and read out by different orders after individually controllable storage times. The qubits are written in by the order 1-2-3 and read out by three different orders 1-2-3, 3-2-1, and 2-1-3. The error bars denote one standard deviation of the corresponding measured values. The solid (dashed) black lines on the measured average fidelities denote the classical bounds on the fidelity with (without) the contribution of the multi-photon component in the input weak coherent pulse. The red solid lines denote the corresponding classical bound by further taking into the contribution of the limited retrieval efficiency.

technique may also find applications in other quantum information systems that require individual addressing and programmable control [31].

In this experiment, we focus on the proof-of-principle demonstration, where the input state, although remaining unknown to the atomic quantum memory, is prepared by the write AODs in the same experimental setup. For future applications, it would be important to store the input state free-propagating from the outside into this random access quantum memory as well. Depending on the type of the optical qubits coming from the outside, this could be done by the AODs or other linear optical devices. For instance, if the input qubit is carried by the time bins of optical pulses, we can program the AODs to split different time-bins into different optical paths in our dual-rail representation so that they can be stored into the corresponding multiplexed atomic memory cells. If the input state is carried by different polarizations of an optical pulse, we can first use a polarizing beam splitter to split them into different paths and then use AODs in those paths for spatial multiplexing. Preparation of different types of optical qubits from the outside, possibly by another atomic ensemble, and demonstration of their storage and control inside the random access quantum memory is an interesting future direction.

Data Availability The data that support the findings of this study are available from the authors upon request.

Acknowledgements: This work was supported by by the Ministry of Education of China and the National key Research and Development Program of China (2016YFA0301902).

Competing interests: The authors declare that there are no competing interests.

Author Information: Correspondence and requests for materials should be addressed to L.M.D. (lmd-uan@tsinghua.edu.cn).

Author Contributions: L.M.D. conceived the experiment and supervised the project. N.J., Y.F.P., W.C., C.L.,

S.Z. carried out the experiment. N. J. and Y. F. P. contribute equally to this experiment. L.M.D., N.J., Y.F.P. wrote the manuscript.

-
- [1] Briegel, H. J., Dur, W. J., Cirac, I. & Zoller, P. Quantum repeaters: the role of imperfect local operations in quantum communication. *Phys. Rev. Lett.* **81**, 5932-5935 (1998).
 - [2] Duan, L.-M., Lukin, M. D., Cirac, J. I. & Zoller, P. Long-distance quantum communication with atomic ensembles and linear optics. *Nature* **414**, 413-418 (2001).
 - [3] Kimble, H. J. The quantum internet. *Nature* **453**, 1023-1030 (2008).
 - [4] Lvovsky, A. I., Tittel, W. & Sanders, B. C. Optical quantum memory. *Nature Photon.* **3**, 706-714 (2009).
 - [5] Hammerer, K., Sørensen, A. S. & Polzik, E. S. Quantum interface between light and atomic ensembles. *Rev. Mod. Phys.* **82**, 1041-1093 (2010).
 - [6] Sangouard, N., Simon, C., de Riedmatten, H. & Gisin, N. Quantum repeaters based on atomic ensembles and linear optics. *Rev. Mod. Phys.* **83**, 33-80 (2011).
 - [7] Collins, O. A., Jenkins, S. D., Kuzmich, A. & Kennedy, T. A. B. Multiplexed memory-insensitive quantum repeaters. *Phys. Rev. Lett.* **98**, 060502 (2007).
 - [8] Knill, E., Lafamme, R. & Milburn, G. A scheme for efficient quantum computation with linear optics. *Nature* **409**, 46-52 (2001).
 - [9] Giovannetti, V., Lloyd, S., Maccone, L. Quantum random access memory. *Phys. Rev. Lett.* **100**, 160501 (2008).
 - [10] Barrett, S. D., Rohde, P. P. & Stace, T. M. Scalable quantum computing with atomic ensembles. *New J. Phys.* **12**, 093032 (2010).
 - [11] Fleischhauer, M., Imamoglu, A. & Marangos, J. P. Electromagnetically induced transparency: Optics in coherent media. *Rev. Mod. Phys.* **77**, 633 (2005).
 - [12] Chou, C.-W. et al. Measurement-induced entanglement for excitation stored in remote atomic ensembles. *Nature* **438**, 828-832 (2005).
 - [13] Chaneliere, T. et al. Storage and retrieval of single photons transmitted between remote quantum memories. *Nature* **438**, 833-836 (2005).
 - [14] Eisaman, M. et al. Electromagnetically induced transparency with tunable single-photon pulses. *Nature* **438**, 837-841 (2005).
 - [15] Julsgaard, B., Sherson, J., Cirac, J. I., Fiurasek, J. & Polzik, E. S. Experimental demonstration of quantum memory for light. *Nature* **432**, 482-486 (2004).
 - [16] Simon, J., Tanji, H., Ghosh, S. & Vuletic, V. Single-photon bus connecting spin-wave quantum memories. *Nat. Phys.* **3**, 765-769 (2007).
 - [17] Lan, S.-Y. et al. A Multiplexed Quantum Memory. *Opt. Express* **17**, 13639-13645 (2009).
 - [18] Dudin, Y. O., Li, L., Kuzmich, A. Light storage on the minute scale. *Phys. Rev. A* **87**, 031801(R) (2013).
 - [19] Yang, S.-J., Wang, X.-J., Bao, X.-H. & Pan, J.-W. An efficient quantum light-matter interface with sub-second lifetime. *Nat. Photon.* **10**, 381-384 (2016).
 - [20] Pu, Y.-F., Jiang, N., Chang, W., Yang, H.-X., Li, C. & Duan, L.-M. Experimental realization of a multiplexed quantum memory with 225 individually accessible memory cells. *Nat. Commun.* **8**, 15359 (2017).
 - [21] Chrapkiewicz, R., Dabrowski, M., Wasilewski, W. High-Capacity Angularly Multiplexed Holographic Memory Operating at the Single-Photon Level. *Phys. Rev. Lett.* **118**, 063603 (2017).
 - [22] Hsiao, Y.-F. et al. Highly Efficient Coherent Optical Memory Based on Electromagnetically Induced Transparency. *Phys. Rev. Lett.* **120**, 183602 (2018).
 - [23] Vernaz-Gris, P., Huang, K., Cao, M., Sheremet, A.-S., Laurat, J. Highly-efficient quantum memory for polarization qubits in a spatially-multiplexed cold atomic ensemble. *Nat. Commun.* **9**, 363 (2018).
 - [24] de Riedmatten, H., Afzelius, M., Staudt, M. U., Simon, C. & Gisin, N. A solid-state light matter interface at the single-photon level. *Nature* **456**, 773-777 (2008).
 - [25] Saglamyurek, E. et al. Broadband waveguide quantum memory for entangled photons. *Nature* **469**, 513-518 (2011).
 - [26] Usmani, I., Afzelius, M., de Riedmatten, H., & Gisin, N. Mapping multiple photonic qubits into and out of a solid-state atomic ensemble. *Nat. Commun.* **1**, 12 (2010).
 - [27] Gundogan, M., Ledingham, P. M., Almasi, A., Cristiani, M., & de Riedmatten, H. Quantum Storage of a Photonic Polarization Qubit in a Solid. *Phys. Rev. Lett.* **108**, 190504 (2012).
 - [28] Tang, J.-S. et al. Storage of multiple single-photon pulses emitted from a quantum dot in a solid-state quantum memory. *Nat. Commun.* **6**, 8652 (2015).
 - [29] Laplane, C., Jobez, P., Etesse, J., Timoney, N., Gisin, N., Afzelius, M. Multiplexed on-demand storage of polarization qubits in a crystal. *New J. Phys.* **18**, 013006 (2016).
 - [30] Bernien, H., et al. Probing many-body dynamics on a 51-atom quantum simulator. *Nature* **551**, 579C584 (2017).
 - [31] Debnath, S., Linke, N. M., Figgatt, C., Landsman, K. A., Wright, K. & Monroe, C. Demonstration of a small programmable quantum computer with atomic qubits. *Nature* **536**, 63-66 (2016).
 - [32] C. Simon, et al. Quantum memories. *Eur. Phys. J. D* **58**, 1C22 (2010).
 - [33] James, D. F. V., Kwiat, P. G., Munro, W. J. & White, A. G. Measurement of qubits. *Phys. Rev. A* **64**, 052312-052326 (2001).

(2001).

- [34] Specht, H. P. *et al*, A single-atom quantum memory *Nature* **473**,190 (2011).
- [35] Gujarati, T.P., Wu, Y., Duan, L.-M., Intrinsic retrieval efficiency for quantum memories: A three-dimensional theory of light interaction with an atomic ensemble *Phys. Rev. A* **97**, 033826 (2011).

SUPPLEMENTARY NOTE

SUPPLEMENTARY NOTE 1: EXPERIMENTAL SETUP

A ^{87}Rb atomic cloud is loaded into a magneto-optical trap (MOT) inside a vacuum glass cell. A strong cooling beam red detuned to the D2 cycling transition $|g\rangle \equiv |5S_{1/2}, F=2\rangle \rightarrow |5P_{3/2}, F'=3\rangle$ by 13 MHz is used for cooling and trapping of the atoms. Some atoms could fall out of the cooling cycle, so we use the repumping laser, resonant to the $|s\rangle \equiv |5S_{1/2}, F=1\rangle \rightarrow |5P_{3/2}, F'=2\rangle$ transition to pump them back. The diameter of the cloud in the MOT is about 3 mm and the temperature is about 300 μK . The atoms are then further cooled by polarization gradient cooling (PGC) for 2 ms. To implement the PGC, we shut off the magnetic gradient coil, increase the red detuning of the cooling laser to 30 MHz, and keep its intensity the same as the value during the MOT loading stage. At the same time, the repumping intensity is decreased to 0.5% of the value at the loading phase. The temperature is then reduced to about 50 μK after the PGC and the size of the MOT remains almost the same. After the atomic state preparation, the optical depth (OD) for the resonance to the $|s\rangle \rightarrow |e\rangle \equiv |5P_{1/2}, F'=2\rangle$ transition reaches a value about 5 at the center of the cloud. During the storage, the ambient magnetic field is not compensated, so the retrieval efficiency of the collective spin-wave excitation undergoes the Larmor precession. The data in Fig.2 and 3 are taken at the time set to the period of the Larmor oscillation. For Fig. 4, the time intervals between the write and the read probe pulses are set to integer multiples of this Larmor period to achieve the highest retrieval efficiency.

We use the electromagnetic-field induced transparency (EIT) scheme to perform the write and the read operations in quantum memory, which convert a probe photon into a collective spin-wave mode at the atomic ground-state manifold by shutting off the control field [1, 2]. The control beam on the $|g\rangle \equiv |5S_{1/2}, F=2\rangle \rightarrow |e\rangle$ has the same circular polarization as the probe beam. The waist diameters of the control beam and the probe beam are 135 μm and 70 μm , respectively, focused on the ensemble and propagating in the forward direction with an angle about 3° between the control and the probe beams. After a controllable storage time, we can retrieve the spin-wave excitation stored in the collective atomic mode by turning on the control field. The retrieved photon is coupled into a single mode fiber for detection. We insert a Fabry-Perot cavity (etalon) in the path of the probe beam before detection to filter out the diffracted control pulse.

SUPPLEMENTARY NOTE 2: MULTIPLEXING AND DEMULTIPLEXING OF OPTICAL CIRCUITS

Crossed acoustic-optical deflectors (AODs) are used in this experiment to control the deflection angles of the laser beam in orthogonal directions by adjusting the radio-frequency (RF) signal inputs to the AODs. We place a pair of AODs in the paths of the control and the write/read probe beams to implement the multiplexing and de-multiplexing optical circuits. Two lens with 20 mm focal length are inserted at the middle point between the atomic ensemble and the write/read AODs, arranged into a $4f$ -configuration (see Fig.1 of the main text. The distance between the atomic ensemble and each side AODs is $2f$, where f is the lens focal length). With the $4f$ -configuration, the laser beams deflected to different angles by the AODs are focused on different corresponding positions of the atomic cloud, enabling individual addressing of each micro-ensemble. The retrieved photon has components coming along different optical paths with stabilized phase difference. We fine tune the directions and positions of the pair of AODs to maintain good interference between different paths for detection in the superposition bases. Only multiplexing AODs are required in the path of the control beam, with no need of de-multiplexing, as shown in Fig. 1 of the main text. The phase differences between different optical paths are intrinsically stable because the deflected beams go through the same apparatus.

No matter which memory cell is addressed in the atomic cloud, the probe beam is required to be coupled into the single-mode fiber at the other side of the atoms for detection of the transmission through all the optical elements. In our experiment, through fine adjustment of the directions and positions of the pair of AODs and lens, we achieve over 65% coupling efficiency for all the 210 optical paths addressing the corresponding memory cells.

We generate the radio-frequency (RF) signal inputs to the AODs by two arbitrary waveform generators (AWG, Tektronix 5014C). We use three channels of each AWG in our experiment. One of the AWG supplies the RF signals for the control, the write, and the read AODs in the X direction, and the other supplies the RF signals of these AODs in the Y direction. The phase differences between the three analog channels of each AWG are precisely controlled. To address one micro-ensemble, the control beam, and the write and the read probe beams need all

to be pointed to the same position of the atomic cloud by adjusting the corresponding RF signal frequencies to control the deflection angles. To address different micro-ensembles, we then scan the frequency of the RF signals for the crossed AODs from 98.8 MHz to 107.2 MHz in step of 0.6 MHz in the X direction, and from 98.8 MHz to 106.6 MHz in step of 0.6 MHz in the Y direction, with the deflected beams pointing to the 15×14 atomic memory cells. The retrieved photons are collected by the de-multiplexing circuit and then coupled into the single mode fiber for detection by a single-photon counter. By programming the AWG to generate arbitrary RF electric signals and their superpositions for the AOD inputs, we can direct the deflected light beams to any paths or their superpositions [3].

SUPPLEMENTARY NOTE 3: CLASSICAL BOUND FOR STATE STORAGE UNDER EXPERIMENTAL IMPERFECTIONS

To confirm genuine quantum storage, we need to demonstrate that the fidelity achieved in the experiment is higher than the classical bound. The classical bound is defined as the best fidelity achievable for the same input pulse if we replace the quantum memory by any classical means. If the input is a single-photon pulse and the input qubit state is uniformly taken from the whole Bloch sphere, the classical bound for the qubit storage fidelity is known to be $2/3$ [4]. In experiments, however, it is difficult to uniformly sample all the possible input qubit states over the whole Bloch sphere. In our experiment, we actually only sample over six complementary input states defined in the main text with equal weights. First, we give an explicit elementary proof that in this case the classical bound is still $2/3$. Then, we take into account the experimental imperfections, in particular the multiphoton components in the input weak coherent pulse and the limited efficiency of the quantum memory, and calculate the classical bound taking into account of all these imperfections. The measured fidelities in the main text are compared with the classical bound that includes contributions of the experimental imperfections to confirm genuine quantum storage.

First, let us explicitly calculate the classical bound under six complementary input states. Assume the best measurement bases are given by $|\psi_+\rangle = \cos(\theta/2)|U\rangle + e^{i\varphi} \sin(\theta/2)|D\rangle$, $|\psi_-\rangle = -\sin(\theta/2)|U\rangle + e^{i\varphi} \cos(\theta/2)|D\rangle$, where θ, φ are to-be-optimized parameters. We calculate the average fidelity over the six input states $|U\rangle, |D\rangle, |\pm\rangle, |\sigma_\pm\rangle$. For the input state $|U\rangle$, we have a probability of $\cos^2(\theta/2)$ ($\sin^2(\theta/2)$) to obtain the outcome $|\psi_+\rangle$ ($|\psi_-\rangle$) which has a fidelity of $\cos^2(\theta/2)$ ($\sin^2(\theta/2)$). The average fidelity is therefore

$$\overline{F}_U = \cos^2 \frac{\theta}{2} \cos^2 \frac{\theta}{2} + \sin^2 \frac{\theta}{2} \sin^2 \frac{\theta}{2}. \quad (1)$$

Similarly, for the input states $|D\rangle, |\pm\rangle, |\sigma_\pm\rangle$, the corresponding fidelities are given respectively by

$$\overline{F}_D = \sin^2 \frac{\theta}{2} \sin^2 \frac{\theta}{2} + \cos^2 \frac{\theta}{2} \cos^2 \frac{\theta}{2}, \quad (2)$$

$$\overline{F}_+ = \frac{1}{4}(\cos \frac{\theta}{2} + e^{i\varphi} \sin \frac{\theta}{2})^2 (\cos \frac{\theta}{2} + e^{i\varphi} \sin \frac{\theta}{2})^2 + \frac{1}{4}(\cos \frac{\theta}{2} - e^{i\varphi} \sin \frac{\theta}{2})^2 (e^{i\varphi} \cos \frac{\theta}{2} - \sin \frac{\theta}{2})^2, \quad (3)$$

$$\overline{F}_- = \frac{1}{4}(\cos \frac{\theta}{2} - e^{i\varphi} \sin \frac{\theta}{2})^2 (\cos \frac{\theta}{2} - e^{i\varphi} \sin \frac{\theta}{2})^2 + \frac{1}{4}(\cos \frac{\theta}{2} + e^{i\varphi} \sin \frac{\theta}{2})^2 (-e^{i\varphi} \cos \frac{\theta}{2} - \sin \frac{\theta}{2})^2, \quad (4)$$

$$\overline{F}_{\sigma_+} = \frac{1}{4}(\cos \frac{\theta}{2} + ie^{i\varphi} \sin \frac{\theta}{2})^2 (\cos \frac{\theta}{2} + ie^{i\varphi} \sin \frac{\theta}{2})^2 + \frac{1}{4}(\cos \frac{\theta}{2} - ie^{i\varphi} \sin \frac{\theta}{2})^2 (-ie^{i\varphi} \cos \frac{\theta}{2} + \sin \frac{\theta}{2})^2, \quad (5)$$

$$\overline{F}_{\sigma_-} = \frac{1}{4}(\cos \frac{\theta}{2} - ie^{i\varphi} \sin \frac{\theta}{2})^2 (\cos \frac{\theta}{2} - ie^{i\varphi} \sin \frac{\theta}{2})^2 + \frac{1}{4}(\cos \frac{\theta}{2} + ie^{i\varphi} \sin \frac{\theta}{2})^2 (ie^{i\varphi} \cos \frac{\theta}{2} + \sin \frac{\theta}{2})^2, \quad (6)$$

The average fidelity over these six complementary input states under equal weights therefore becomes

$$\overline{F} = \frac{1}{6}(\overline{F}_U + \overline{F}_D + \overline{F}_+ + \overline{F}_- + \overline{F}_{\sigma_+} + \overline{F}_{\sigma_-}) = \frac{2}{3}. \quad (7)$$

Now we discuss the classical bound when the input is a weak coherent pulse. It has been known that for a state containing N qubits, the best classical strategy leads to a fidelity of $F = \frac{N+1}{N+2}$ [5]. For an input coherent state with a

mean photon number μ , the number of photons (optical qubits) n satisfy the Poissonian distribution $P(\mu, n) = e^{-\mu} \frac{\mu^n}{n!}$. Then, the maximum achievable fidelity becomes a weighted sum over n of the fidelity for a given n where the weight is given by the Poissonian distribution [6]. Combining the above two results together, the average input-output fidelity is simply the statistical mixture of the fidelities for $n \geq 1$ photons [7]:

$$F(\mu) = \sum_{n=1}^{+\infty} \frac{n+1}{n+2} \frac{P(\mu, n)}{1 - P(\mu, 0)} \quad (8)$$

$$= \frac{1}{1 - e^{-\mu}} \left[\frac{1 - e^{-\mu} - \mu + \mu^2}{\mu^2} - \frac{e^{-\mu}}{2} \right], \quad (9)$$

This bound gives a value of 68.8% for our experimental case with the mean photon number $\mu \simeq 0.5$ for the input weak coherent pulse.

Finally, we need to consider the case when the retrieval efficiency η is significantly less than 1. In this case, the classical memory protocol could use a more elaborate strategy to take advantage of the finite retrieval inefficiency to achieve a higher average fidelity when the detector successfully registers an output photon. As shown in Refs. [7], the average state fidelity conditional on a successful registration of the output photon has the expression

$$F(\mu, \eta) = \frac{\frac{n_{min}+1}{n_{min}+2}\gamma + \sum_{n \geq n_{min}} \frac{n+1}{n+2} P(\mu, n)}{\gamma + \sum_{n \geq n_{min}} P(\mu, n)}, \quad (10)$$

where $0 < \gamma < P(\mu, n_{min})$ is a parameter that is adjusted to mimic the memory efficiency η , and n_{min} is the cutoff photon number to be optimized to get the highest bound $F(\mu, \eta)$. The supplementary information of Ref. [7] explains how to calculate the parameter γ in detail with a given retrieval efficiency η . The effective classical efficiency η_C is defined as the probability that the classical device gives an output qubit,

$$\eta_C = \frac{\gamma + \sum_{n \geq n_{min}} P(\mu, n)}{1 - P(\mu, 0)},$$

Here, the η_C is assumed to be the same as the retrieval efficiency η , and n_{min} is obtained as follows [7]

$$n_{min} = \min_i \sum_{n \geq i+1} P(\mu, n) \leq (1 - P(\mu, 0))\eta.$$

For our experimental data on the retrieval efficiency, the corresponding classical bounds are shown in Fig. 3b of the main text and our measured quantum efficiencies for the memory cells still exceed the corresponding classical bounds taking into account of these experimental imperfections.

SUPPLEMENTARY NOTE 4: STANDARD DEVIATION OF STORAGE FIDELITIES FOR EVERY MEMORY CELLS

For each pair of the memory cells, we measured the storage fidelity F under six complementary input states, and the results are shown in maintext for all the 105 pairs of memory cells. Here we show the corresponding standard deviations of the average fidelity in Fig. 5 for all the 105 pairs of memory cells. The standard deviations of averaged fidelities from the six measurements with equal weight, are all below 2%.

-
- [1] Eisaman, M. et al. Electromagnetically induced transparency with tunable single-photon pulses. *Nature* **438**, 837-841 (2005).
 - [2] Julsgaard, B., Sherson, J., Cirac, J. I., Fiurasek, J. & Polzik, E. S. Experimental demonstration of quantum memory for light. *Nature* **432**, 482-486 (2004).
 - [3] Pu, Y.-F., Jiang, N., Chang, W., Yang, H.-X., Li, C. & Duan, L.-M. Experimental realization of a multiplexed quantum memory with 225 individually accessible memory cells. *Nat. Commun.* **8**, 15359 (2017).
 - [4] Michael, A. N., Isaac, L. Chuang. The postulates of quantum mechanics In *Quantum Computation And Quantum Information* Published in the United States of America by Cambridge University Press, New York, (2000). P.80-90
 - [5] Massar, S., Popescu, S. Optimal Extraction of Information from Finite Quantum Ensembles *Phys. Rev. Lett* **74**, 1259 (1995).
 - [6] Specht, H. P. *et al*, A single-atom quantum memory *Nature* **473**, 190 (2011).
 - [7] Gundogan, M., P. M. Ledingham, P. M., Almasi, A., Cristiani, M., H. de Riedmatten, H., Quantum Storage of a Photonic Polarization Qubit in a Solid. *Phys. Rev. Lett.* **108**, 190504 (2012).

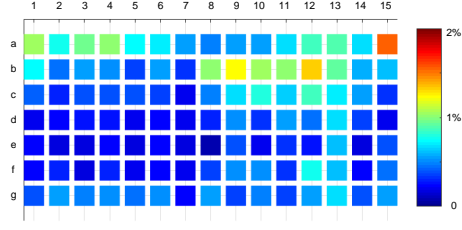


FIG. 5: Measured standard deviations of the average fidelities of the retrieved optical qubits after storage in the 210-cell quantum memory. The standard deviations of the corresponding measured average fidelities (see Fig. 2c in the maintext) for the six complementary input states of optical qubits after a $1.38 \mu s$ storage time